Coffee waste-derived biochar as a flame retardant for epoxy nanocomposites

Sustainable Materials and Technologies 41 (2024) e01079

Contents lists available at ScienceDirect

Sustainable Materials and Technologies

journal homepage: www.elsevier.com/locate/susmat

Coffee waste-derived biochar as a flame retardant for epoxy nanocomposites

Aurelio Bifulco [a,*], Mattia Bartoli [b,c,d], Immacolata Climaco [a], Maria Cristina Franchino [a], Daniele Battegazzore [e], Rhoda Afriyie Mensah [f], Oisik Das [f], Henri Vahabi [g], Giulio Malucelli [e], Antonio Aronne [a], Claudio Imparato [a,*]

[a] Department of Chemical, Materials and Production Engineering, University of Naples Federico II, 80125 Naples, Italy
[b] Center for Sustainable Future Technologies–CSFT@POLITO, 10144 Turin, Italy
[c] Consorzio Interuniversitario Nazionale per la Scienza e Tecnologia dei Materiali (INSTM), 50121 Florence, Italy
[d] Department of Applied Science and Technology, Politecnico di Torino, 10129 Turin, Italy
[e] Department of Applied Science and Technology, Politecnico di Torino, 15121 Alessandria, Italy
[f] Division of Structural and Fire Engineering, Department of Civil, Environmental, and Natural Resources Engineering, Luleå University of Technology, Luleå, 97187, Sweden
[g] Université de Lorraine, CentraleSupélec, LMOPS, Metz F-57000, France

ARTICLE INFO

Keywords:
Epoxy resin
Spent coffee grounds
Ternary oxide
Sol-gel
Flame retardancy
Forced-combustion behavior

ABSTRACT

Starting from spent coffee grounds, the use of coffee-derived biochar (CB) as a flame retardant (FR) additive was explored following a waste-to-wealth approach. CB was employed alone and in combination with ammonium polyphosphate (APP) and a ternary (Si-Ti-Mg) mixed oxide to enhance the thermal, fire, and mechanical performances of a bisphenol A diglycidyl ether (DGEBA)-based epoxy resin modified with (3-aminopropyl)-triethoxysilane (APTES) and cured with a cycloaliphatic amine hardener. The presence of silicon-modified epoxy chains guaranteed the uniform distribution of CB throughout the resin. The combined FR action of fillers (CB, APP, and Si-Ti-Mg oxide) and the acidic characteristics of hybrid epoxy moieties enabled the achievement of a no dripping UL 94-V-0 classification for epoxy resin containing 20 wt% CB and 1 wt% of phosphorus loading, significantly increasing the flexural modulus (by ~15%). Although it is not self-extinguishing, compared to pristine resin, the silicon-modified epoxy nanocomposite filled only with CB exhibited a remarkable decrease in the peak of heat release rate (pHRR) (by ~65%) and a beneficial smoke suppressant effect with a notable decrease (~11%) in the total smoke production. Cone calorimetry tests, pyrolysis combustion flow calorimetry analysis, and microscopy measurements helped to outline the combined mode of action of CB, APP, and Si-Ti-Mg oxide in the flame retardation of the hybrid epoxy resin, highlighting a strong FR action in the condensed phase, with the formation of a stable aromatic ceramic char, as well as the smoke suppressant character due to the basic nature of the ternary metal oxide and the ability of porous biochar to adsorb the generated gases.

1. Introduction

The use of polymeric materials is undeniable in our daily life, where high-performance applications demand a growing amount of low-flammable polymer-based products with excellent mechanical properties [1,2]. On the other hand, the huge production of polymeric wastes is one of the major concerns in modern society, as their improper management is causing problems to the environment and human health, such as groundwater contamination and the release of toxic gases, especially due to additives [3]. To face these issues, governments and the scientific community are promoting the transition to a circular economy model, and the development of more valorization technologies and sustainable approaches [4]. Epoxy resins exhibit good mechanical behavior, chemical resistance, and thermal stability and thus are largely employed in the transportation industry, though their flame retardation is often needed to fulfill specific standards [5]. Although halogen-based flame retardants (HFRs) are highly effective in improving the fire behavior of epoxy composites, recent regulations have definitively

* Corresponding authors.
E-mail addresses: aurelio.bifulco@unina.it (A. Bifulco), claudio.imparato@unina.it (C. Imparato).

https://doi.org/10.1016/j.susmat.2024.e01079
Received 7 June 2024; Received in revised form 23 July 2024; Accepted 6 August 2024

banned many of them in the European Union, due to the adverse consequences linked to the recycling of wastes containing such compounds [1]. Phosphorus (P)-based FRs (e.g., ammonium polyphosphate (APP), phytic acid, bio-based phosphaphenanthrene-derived anhydride) can be considered a greener alternative to HFRs, as they allow for the synthesis of more sustainable epoxy systems (e.g., vitrimers) and their flame retardant action does not involve the generation of harmful gases [6–10]. However, unlike HFRs, large amounts of P-based FRs (i.e., with 2, 3 wt% P) are needed in the epoxy matrix to achieve satisfactory performances; further, synergistic effects are often required to keep the flame retardant loading as low as possible [11]. Silica and metal oxides with acidic and basic sites on their surface can work as char promoters and barriers toward heat and oxygen transfer during the combustion of the epoxy matrix [12–14]. Natural metal silicates (e.g., clays) and synthetic nanostructures containing metal ions, such as titanium or magnesium, have been shown to provide increased charring or smoke suppression, besides physical barrier effects [15–17]. The use of naturally-occurring additives (e.g., lanosol, phytic acid, chitosan) [18,19] and functional biowastes (e.g., humic acid, lignin, tannic acid) [20], in combination with P-based FRs, allows for reducing the required concentration of P-containing additives and consequently the depletion of phosphorus, giving at the same time added value to waste materials. For example, Venezia et al. prepared self-extinguishing epoxy composites based on Bisphenol A diglycidyl ether (DGEBA) cured with isophorone diamine (IDA), a cycloaliphatic hardener, using 6 wt% of humic acid in combination with urea and APP. Aliphatic curing agents are less toxic than aromatic ones but more flammable, which makes the flame retardancy of aliphatic epoxy systems full of hurdles [21]. The exploitation of humic acid was crucial to achieve no dripping UL 94-V-0 rating and a strong decrease in the peak of heat release rate (pHRR) up to 21%, even with only 1 wt% of P loading and no detrimental effects on the mechanical performances [22].

Among the biowastes available from the food industry, the by-products of coffee processing, i.e. coffee pulp, husks, silverskin, and spent coffee grounds (SCGs), represent a largely unexploited resource [23]. 650 kg of SCGs are obtained from 1 ton of green coffee SCGs during instant coffee making and beverage preparation, with an annual production rate of around 6 million tons worldwide [24]. The surface chemistry of SCGs, rich in hydroxyl groups, makes this biowaste suitable for use as a functional FR in epoxy resins [25]. Vahabi et al. modified SCGs with dimethyl phosphite (P-coffee) and employed them to provide a DGEBA resin cured by a cycloaliphatic hardener with low flammability in horizontal flame spread tests and 40% reduction in pHRR compared to the virgin sample using 30 wt% of P-coffee [26]. Yang et al. investigated the influence of SCGs' size on the fire behavior and mechanical properties of a resin mixture diluted with 1,2,3-propanetriol glycidyl ether and cured with IDA, m-xylylenediamine, and 2,2,4-trimethylhexane-1,6-diamine. Compared to the pristine system, the final product containing 30 wt% of SCGs showed a decrease in pHRR and total heat release of 52 and 34%, respectively [27].

The pyrolytic conversion of SCGs in a range of temperatures between 500 and 800 °C allows for the production of a coffee biochar (CB) showing excellent dispersibility in epoxy resins, superior thermal stability, and high porosity, lessening the variability due to different SCGs sources. Due to these peculiarities, Bartoli et al. used CB as a filler to improve the electrical performances of epoxy composites and observed that the change in the operative conditions in the production of CB led to epoxy products with different electrical conductivities, reaching four orders of magnitude higher values than that of samples filled with carbon black [28]. The uniform dispersion of CB throughout the polymer matrix also improved the mechanical behavior, with respect to the unmodified resin. Alhelal et al. prepared epoxy composites through 3D printing technology at two different concentrations of CB. In comparison with pristine resin, 1 wt% of CB led to an increase of storage modulus, flexural modulus and strength up to 27.5, 56 and 43%, respectively, whereas 3 wt% of CB caused the formation of agglomerates in the polymer network and negatively impacted on both viscoelastic and flexural properties [29].

In general, biochar is gaining interest as a bio-derived and cheap filler able to remove trace contaminants from wastewater [30] and enhance the mechanical, thermal, and fire performances of thermoset composites [31–33]; however, the study of biochar obtained from SCGs as a flame retardant in epoxy systems is lacking in the recent scientific literature. Nevertheless, the high graphitization degree of CB and its physico-chemical features make it a very promising material for the manufacture of flame retardant epoxy composites.

In this research work, self-extinguishing DGEBA-based epoxy composites, containing unmodified CB as an effective flame retardant and cured with IDA as a cycloaliphatic hardener, were obtained. To improve the dispersion of CB into the epoxy matrix, DGEBA was modified by reaction with a coupling agent, i.e., 3-aminopropyltriethoxysilane (APTES). CB was incorporated into the hybrid silicon-modified epoxy matrix in combination with a ternary (Si-Ti-Mg) mixed oxide, containing titanium and magnesium species in a silicate matrix, prepared by a convenient and sustainable sol-gel route, and APP as a source of phosphorus. The thermal and viscoelastic properties of epoxy composites were studied by thermogravimetric analysis and dynamic mechanical thermal analysis, respectively. The influence of CB and Si-Ti-Mg oxide on the fire behavior of epoxy systems was thoroughly investigated by pyrolysis flow combustion calorimetry and cone calorimetry tests. Finally, scanning electron microscopy images with energy-dispersive X-ray analysis of residual chars concurred to shed light on the flame retardant mechanisms taking place during the burning process. This research demonstrates a feasible and sustainable approach to effectively use a biowaste as a functional flame retardant additive in epoxy composites, hence fulfilling the circular economy approach.

2. Experimental

2.1. Preparation of coffee biochar

Coffee biochar (CB) was produced by pyrolysis of spent coffee grounds (SCGs, Arabica mixture) collected from Katia Cafè (Turin, Italy) and supplied by Casa del Caffè Vergnano S.p.A. (Turin, Italy). First, SCGs were dried at 105 °C for 72 h in a ventilated oven. Dried SCGs were pyrolyzed in a steel vessel using a tubular furnace (Carbolite TZF 12/65/550, Neuhausen, Germany) with a nitrogen flux (4 mL/min) and a heating rate of 10 °C/min, keeping the systems at the maximum temperature of 800 °C for 30 min. CB was used without further purification. The average particle size of the so-obtained CB was about 100 μm; after 2 h ball milling (carried out in a 700 cm^3 Turbula T-2C mixer (Willy A. Bachofen AG, Muttenz, Switzerland)) equipped with eight zirconium balls, the average size further decreased (see section 3.1).

2.2. Synthesis of Si-Ti-Mg mixed oxide

A silicon-titanium-magnesium mixed oxide was synthesized by sol-gel method using tetraethyl orthosilicate (TEOS, 99%), titanium (IV) isopropoxide ($Ti(i\text{-}OPr)_4$, 97%) and magnesium ethoxide ($Mg(OEt)_2$, >98%) as precursors, diethanolamine (dea, 98%) as complexing agent, acetic acid (AcOH, 99%) as catalyst, and ethanol as solvent. The sol-gel technique was chosen because it allows the preparation of multinary oxides with a homogeneous dispersion of the components, operating in mild conditions. The adopted procedure is sketched in Fig. S1. More in detail, 1.7 g of $Mg(EtO)_2$ were dissolved in 35 mL of EtOH and 0.70 mL of dea (dea/Mg molar ratio = 0.5) under stirring at 50 °C. Then, 10.0 mL of TEOS was added, followed by a second solution containing 4.5 mL of $Ti(i\text{-}OPr)_4$, 5.0 mL of EtOH, and 0.70 mL of dea (dea/Ti molar ratio = 0.5). The resulting dark orange solution was left under stirring for 30 min. Acetic acid (3.5 mL) was then added to the mixture, lowering its pH from 10.8 to about 5.9, to favor the hydrolysis of TEOS (the less reactive of the three precursors) and the subsequent growth of an interconnected

oxide network, aided by the slightly acidic pH and the complexing ability of acetate. The system was cooled down to room temperature and then bidistilled water was added (2.7 mL), split into four fractions slowly incorporated within 2 h, to moderate the hydrolysis and condensation rates. The molar ratios Si:Ti:Mg:dea:AcOH:H_2O were 0.6:0.2:0.2:0.2:0.8:2.0. The mixture was left stirring overnight until a homogeneous light brown gel formed (Fig. S2). After 1 day of aging, the gel was dried between 80 and 120 °C, and the xerogel was finally ground by ball milling to obtain a fine powder. The nominal composition of the Si-Ti-Mg oxide is reported in Table S1.

2.3. Preparation of hybrid epoxy composites

An epoxy system (SX10) composed of Bisphenol A diglycidyl ether (DGEBA) and isophorone diamine (IDA, SX10), a cycloaliphatic diamine hardener, were purchased from MATES S.r.l. (Milan, Italy) and used as received. (3-aminopropyl)-triethoxysilane (APTES, N98%) and ammonium polyphosphate (APP) were acquired from Sigma-Aldrich (St. Louis, USA). In a typical procedure, APTES (7 wt%, i.e., the minimum concentration to obtain a uniform dispersion of CB in the polymer matrix, see Fig. S3) was added to DGEBA under stirring at room temperature. Then, proper amounts of CB, APP, and Si-Ti-Mg oxide (see Table 1) were added, and the mixture was ultrasonicated by using a Q500 tip sonicator (QSonica) with an output power of 150 W for 1 min at 40 Hz. The formation of APTES-modified epoxy chains is usually performed by mixing the resin and the coupling agent at 80 °C for about 2 h [22,34]; however, in our case, it was accomplished in a much shorter time without the need for prolonged heating, as indicated by the excellent CB dispersion (Fig. S3), owing to the ultrasonication step, which provides energy by cavitation to the system with limited heating. This approach is a practical way to obtain uniform nanocomposites through a less energy- and time-consuming manufacturing process. Then, the system was cooled down to room temperature and IDA (26 w/w% with respect to DGEBA) was added. After pouring in the mold, the system was cured at 60 °C for 12 h and finally post-cured at 80 °C for 4 h. The whole procedure is presented in Scheme 1.

The composition of all the prepared thermosets is reported in Table 1. The samples' codes include: "E" for epoxy resin, "Si" for APTES, "C" for biochar, "T" for ternary (Si-Ti-Mg) oxide, "A" for APP, and "1P" or "0.5P" to indicate the wt% of P.

2.4. Characterization techniques

Raman spectra were collected using a Renishaw inVia Apparatus (H43662, Gloucestershire, UK) equipped with a laser line (wavelength of 532 nm) in the range from 500 to 3500 cm^{-1}. The deconvolution of signals was performed with a Matlab® (version R2020a) homemade compiled software according to Tagliaferro et al. [35].

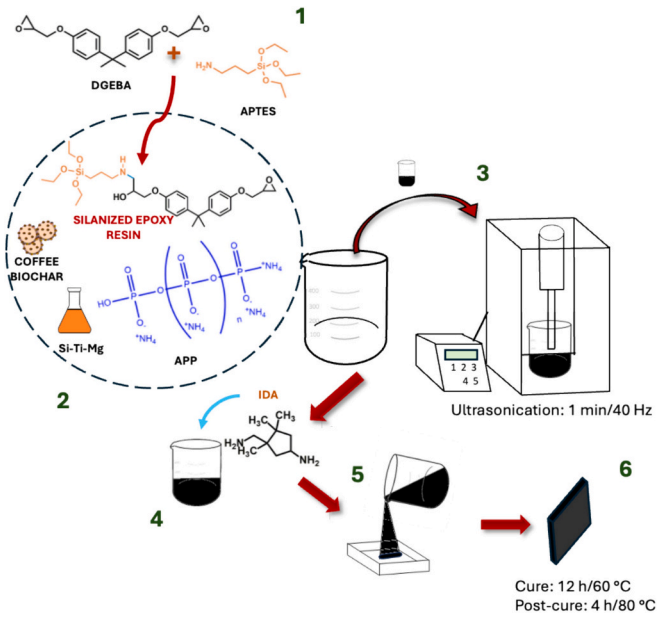

Scheme 1. Synthesis procedure of hybrid epoxy composites: (1) reaction of DGEBA with APTES to give silanized epoxy molecules; (2) hybrid resin and additives; (3) mixing and ultrasonication; (4) addition of IDA hardener; (5) pouring in the molds; (6) curing and post-curing.

The morphology and chemical composition of CB, the hybrid nanocomposites containing all the fillers (ternary oxide, CB, and APP), and residual chars obtained from UL 94 vertical flame spread tests were investigated by employing a **Field Emission Scanning Electron Microscope** (FESEM, Zeiss SupraTM40, Oberkochen, Germany), equipped with an **Energy Dispersive X-ray** detector (EDX, Oxford Inca Energy 450, Oberkochen, Germany).

Fourier Transform InfraRed (FTIR) spectra were collected by attenuated total reflectance (ATR) mode (Nicolet 5700, Thermoscientific, Waltham, MA, USA equipped with a Smartorbit, Thermoscientific, Waltham, MA, USA) in the range from 500 to 4000 cm^{-1}. The IR transmittance spectra of powders mixed in KBr pellets were collected

Table 1
Composition of the studied epoxy-based samples.

Sample	DGEBA (wt%) [a]	APTES (wt%) [a]	CB (wt%) [a]	Si-Ti-Mg (wt%) [a]	APP (wt%) [a]	IDA (wt%) [a]	TOT [b] (wt%) [a]	P (wt%) [a]
E	79.4	–	–	–	–	20.6	–	–
EC	79.4	–	20	–	–	20.6	20	–
ET	79.4	–	–	14	–	20.6	14	–
EA1P	79.4	–	–	–	3	20.6	3	1.0
ECA1P	79.4	–	20	–	3	20.6	23	1.0
ETC	79.4	–	20	14	–	20.6	34	–
ETA1P	79.4	–	–	14	3	20.6	17	1.0
ETAC1P	79.4	–	20	14	3	20.6	37	1.0
ESi	79.4	7	–	–	–	20.6	–	–
ESiC	79.4	7	20	–	–	20.6	20	–
ESiT	79.4	7	–	14	–	20.6	14	–
ESiA1P	79.4	7	–	–	3	20.6	3	1.0
ESiCA1P	79.4	7	20	–	3	20.6	23	1.0
ESiTC	79.4	7	20	14	–	20.6	34	–
ESiTA1P	79.4	7	–	14	3	20.6	17	1.0
ESiTAC0.5P	79.4	7	10	7	1.5	20.6	18.5	0.5
ESiTAC1P	79.4	7	20	14	3	20.6	37	1.0

[a] mass percentage referred to (DGEBA+IDA) basis.
[b] total mass percentage of additives.

as the sum of 32 scans with a resolution of 2 cm^{-1}.

The structure of gel-derived Si-Ti-Mg oxide was characterized by **X-ray diffraction (XRD)**, using a Philips PW 3170 X'PERT Pro diffractometer (Philips Analytical, Almelo, The Netherlands) with monochromatized CuKα radiation (40 mA, 40 kV) at a step width of 0.013°, and by FTIR spectroscopy, using a Nicolet 5700 spectrometer (Thermo Fisher, Waltham, MA, USA) with a DTGS KBr detector.

The epoxy-based composites were first analyzed by FTIR spectroscopy, using the abovementioned spectrometer, recording the spectra with 32 scans and a resolution of 4 cm^{-1}. Their thermal behavior was assessed by **thermogravimetric analysis (TGA)**, performed with a SDT Q600 thermoanalyser (TA Instruments, New Castle, DE, USA), heating in nitrogen or air with a flow of 100 mL/min, in the range from 25 to 800 °C at 10 °C/min rate, and **differential scanning calorimetry (DSC)**, by means of a DSC 214 Polyma instrument (NETZSCH-Gerätebau GmbH, Selb, Germany). The measurements were performed under nitrogen flow, heating up to 200 °C at 10 °C/min rate, cooling down, and repeating a second heating step.

The viscoelastic behavior of the materials was assessed through **dynamic mechanical analysis** by using a Q800 dynamic mechanical analyzer by TA Instruments (New Castle, DE, USA), in single cantilever mode, employing 10 × 3 mm^2 section specimens. Tests during a heating ramp were carried out from RT to 150 °C at a heating rate of 3 °C/min, strain of 0.05%, and frequency of 1 Hz.

The **flexural properties** of the samples were performed at room temperature using an Instron® 5966 (Norwood, MA, USA) equipped with a 2 kN load cell and a three-point bending clamp set at 32 mm of span. The deflection speed was set at 1 mm/min. Three specimens (dimensions 10 × 50 × 3 mm^3) were used for each formulation, and the average values and corresponding standard deviations of the flexural modulus ($\mathbf{E_B}$), maximum strength ($\boldsymbol{\sigma_{u,B}}$) and elongation at break ($\boldsymbol{\varepsilon_{f,B}}$) were calculated and reported.

The **flammability** of all epoxy nanocomposites was assessed by UL 94 vertical flame spread tests (IEC 60695–11-10; sample dimensions: 13 × 125 × 3 mm^3).

Limiting oxygen index (LOI) tests were carried out by using a FIRE oxygen index apparatus according to the ASTM D2863 standard.

Cone calorimetry (CC) tests were conducted on the hybrid epoxy composites and neat epoxy samples for comparison. Before testing, the samples were prepared by cutting into dimensions of 100 × 100 × 3 mm^3. The experiments followed the guidelines in ISO 5660 standards and were performed using a Netzsch TCC 918 cone calorimeter. Each specimen was exposed to a heat flux of 50 kWm^{-2}. To ensure reliability, the tests were replicated three times for each formulation to estimate the time to ignition (TTI, s), time to flame out (TTFO, s), total heat release (THR, MJ/m^2), heat release rate (HRR, kW/m^2), peak of heat release rate (pHRR, kW/m^2), total smoke release (TSR, m^2/m^2), total smoke production (TSP, m^2), smoke production rate (SPR, m^2/s), specific extinction area (SEA, m^2/kg), carbon monoxide and carbon dioxide yields (kg/kg).

Flame retardant index (FRI) was calculated using Eq. (1) [36,37]. This index is calculated using the cone calorimeter data of pristine epoxy resin (E) and some of the flame retardant composites developed in this work (Table 1).

$$FRI = \frac{\left[THR \cdot \left(\frac{pHHR}{TTI}\right)\right]_{Neat\ Polymer}}{\left[THR \cdot \left(\frac{pHHR}{TTI}\right)\right]_{Composite}} \quad (1)$$

Pyrolysis combustion flow calorimetry (PCFC) tests were also carried out on the hybrid epoxy composites and neat epoxy samples using a microcalorimeter from Fire Testing Technology, Germany. The samples, weighing between 5 and 8 mg, underwent thermal degradation following the so-called Method A. This method involves the heating of the samples in a pyrolyser, from 100 to 700 °C, in the presence of nitrogen (flow rate: 80 cc/min). The effluent resulting from degradation is combusted in an oxygen environment at 900 °C and a flow rate of 20 cc/min. The samples were subjected to a heating rate of 1 °C/min throughout the tests. The experimental procedures adhered to the specifications in the ASTM D7309–19 standard.

3. Results and discussion

3.1. Chemical and structural characterization of coffee biochar, ternary oxide, and epoxy-based nanocomposites

The FTIR spectrum of SCGs (Fig. 1a) shows the presence of several bands including $\nu_{(O\text{-}H)}$ in the range of 3000–3500 cm^{-1}, as well as $\nu_{(C\text{-}H)}$ in the range from 2800 to 2975 cm^{-1}, in agreement with the presence of polysaccharides. Furthermore, the $\nu_{(C=O)}$ centered at 1713 cm^{-1} suggests the presence of carboxylic-rich species, rising from the torrefaction and extraction processes of raw coffee powders. The CB spectrum (Fig. 1a) displays a simpler pattern with a broad absorption band, due to the carbonaceous matrix, and a weak one centered at around 1000 cm^{-1}, related to the skeletal vibration of CB itself ($\nu_{(C\text{-}O)}$ and $\nu_{(C\text{-}C)}$). The Raman spectrum of CB (Fig. 1b) shows intense D and G peaks and not well-resolved 2D region, suggesting the presence of not highly graphitic carbon, in agreement with the I_D/I_G ratio of 1.7. According to Tuinstra and Koenig [38], the I_D/I_G ratio was used to calculate the average volume of graphitic clusters, which was up to 24 Å. The FESEM analysis of CB (Fig. 1c) reveals a sponge-like structure with a diffuse micrometer-sized porous network throughout the overall structure.

The ternary Si-Ti-Mg oxide was designed as a multivalent additive to assist CB in the improvement of thermal stability and fire resistance of the epoxy resin. Silica is commonly employed in flame retardancy, since, during combustion, it generates a ceramic protective layer that hinders the heat exchange and oxygen diffusion [39]. Titanium oxide can promote char formation because of its acidity [16], while magnesium hydroxide is a widely used flame retardant because its dehydration, occurring at rather low temperatures, absorbs heat and releases water vapor (exploiting the so-called "sink effect") [15,40]. Moreover, both MgO and TiO_2 may contribute to the formation of a dense ceramic barrier and reduce smoke production [12,41]. A uniform dispersion of titanium and magnesium species in the porous silica gel matrix was obtained through the sol-gel procedure adopted. The higher electropositivity of Mg and Ti with respect to Si promotes faster hydrolysis rates of the two metal alkoxides than TEOS [42]. The addition of dea, an effective complexing agent for both Mg and Ti, along with acetic acid, makes easier the control of the hydrolysis rate of their precursors [43,44], favoring the cross-condensation of the three components and the formation of a chemical gel. The amorphous structure of the dried gel powders, attested by XRD (Fig. S4a), indicates the absence of unreacted precursors or segregated crystalline phases. The FTIR spectrum of the material (Fig. S4b) shows a wide asymmetric $\nu_{(Si\text{-}O)}$ band centered at 1080 cm^{-1}, which confirms the formation of a SiO_2 network. The $\nu_{(Si\text{–}O)}$ shoulder at 950 cm^{-1} is associated with Si–O–Ti(Mg) bridges in mixed oxides [45,46], while the bands below 700 cm^{-1} are ascribed to $\nu_{(Ti\text{–}O)}$ and $\nu_{(Mg\text{–}O)}$ [42]. However, although the presence of a $Mg(OH)_2$ phase is not clearly detectable from XRD or FTIR data, the hydrolytic sol-gel process at low temperature is likely to produce magnesium hydroxide clusters or strongly hydroxylated MgO [47,48]. The formation of mixed oxo-hydroxo species probably occurs in the adopted synthesis conditions, as supported by the intense and broad band in the 3700–2900 cm^{-1} range ($\nu_{(O\text{-}H)}$), indicative of hydroxyl groups involved in H-bonds of different strength [46]. The well-known acidic character of TiO_2, given by both the Lewis acidity of Ti^{4+} ions and the moderate Brønsted acidity of Ti-OH groups, was demonstrated to be enhanced by the dispersion of Ti in a silica matrix [49]. The dried gel was not further thermally treated, to preserve its high hydroxylation degree and porous microstructure, also making the synthesis process less energy consuming. As a consequence, residues of the organics added during the

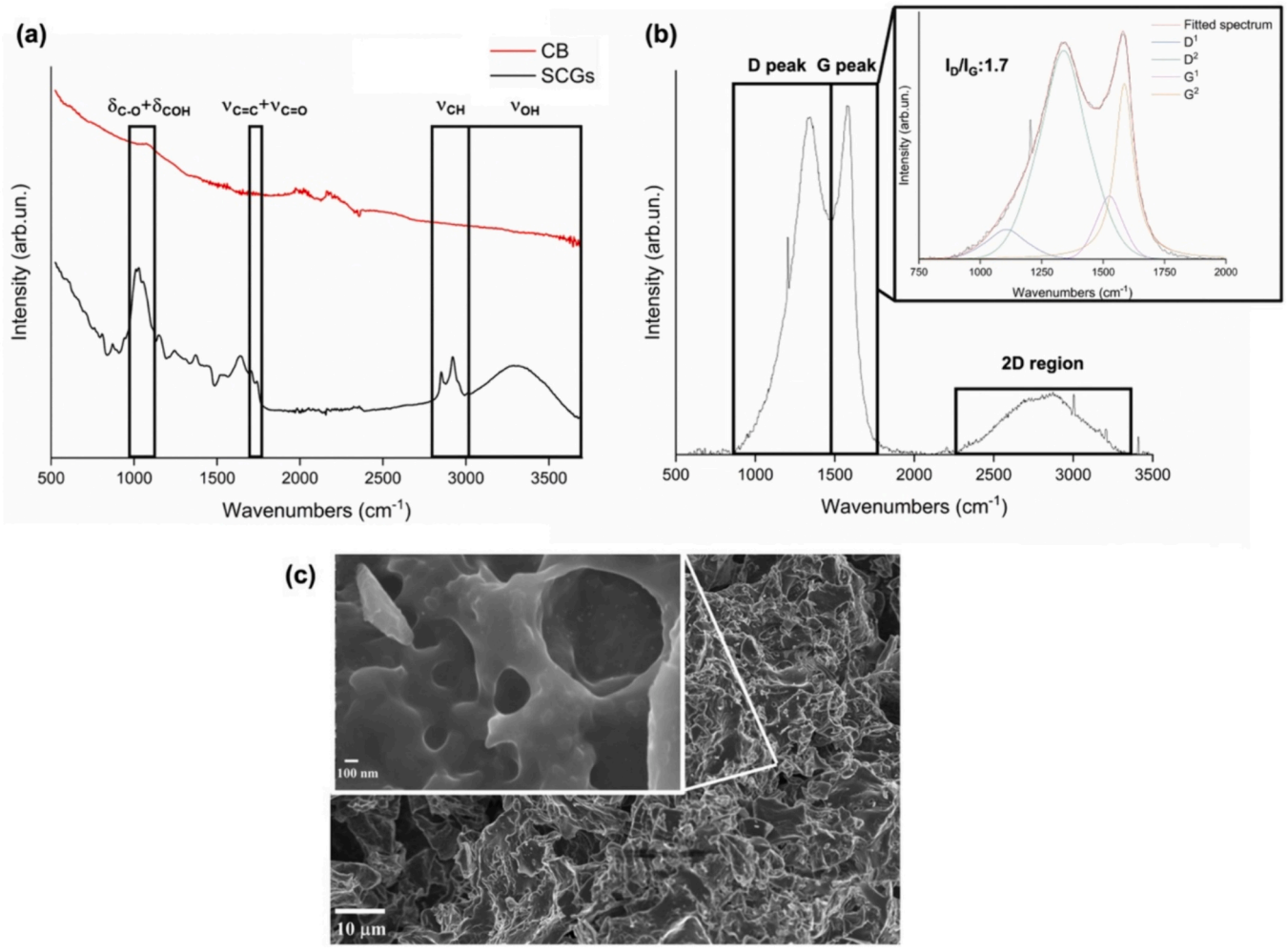

Fig. 1. Characterization of CB: FTIR spectra of SCGs and CB (a), Raman spectrum of CB (b), and FESEM capture of CB (c).

sol-gel procedure are retained in the powders, as indicated by the IR bands at about 1620 and 1430 cm^{-1}, which are compatible with stretching vibrations in carboxylate groups of acetate involved in the coordination of Ti^{4+} or Mg^{2+} ions [50] and N-H bending of dea molecules. On the other hand, some diethanolamine retained in the solid might act as a nitrogen source during the combustion of composites containing Si-Ti-Mg.

In the design of epoxy composites, a coupling agent, such as APTES, is often added to enhance the mixing and dispersion of the fillers by improving the chemical affinity between them and the polymer matrix [17,51]. The modification of DGEBA with APTES through the reaction of oxirane rings with amino groups of the silane originates hybrid epoxy molecules with a rather polar moiety, with ethoxide groups that are easily hydrolyzed, favoring the interaction with other polar species. The advantage of APTES addition on the dispersion of CB particles is evident at visual inspection (see the photographs in Fig. S3), as a sample prepared without silane (EC) contains large heterogeneous aggregates of CB, while ESiC has a uniform appearance and color, showing an even distribution of the filler. The following discussion is therefore focused on epoxy composites prepared with APTES, although the silane-free counterparts were also tested in terms of flammability to verify the role of compatibilization on flame retardant performances.

Fig. S5a shows a typical FESEM image of ESiTAC1P (cross-section fractured in liquid nitrogen): CB particles are quite well homogenously dispersed in the polymer matrix; their average size, as assessed by FESEM, is around (7.8 ± 1.1) µm. In addition, the maps of Si, Ti, Mg, and P (Fig. S5b) clearly indicate a uniform distribution of the ternary oxide and APP in the epoxy network.

The FTIR spectra of representative samples are shown in Fig. S6, where the main vibrations of the epoxy resin are indicated. The completeness of the curing reaction for all the investigated formulations through oxirane ring opening by amino groups is confirmed by the disappearance of the band at 916 cm^{-1}, the most intense peak related to the oxirane ring, and the rise of the O-H stretching band around 3450 cm^{-1}, due to the hydroxyl groups resulting from the reaction. The intensity of the latter band increases with the addition of APTES (ESi sample), suggesting that silanols are formed in the silicon-modified epoxy molecules by the hydrolysis of ethoxide groups. Then, silanols can partially condense generating silica nanostructures [51]. The resulting inorganic-organic hybrid epoxy chains can establish H-bonding interactions with both CB and Si-Ti-Mg oxide, favoring the formation of a well-developed interface between the matrix and the fillers (Scheme 2). In the spectra of the composites, no significant changes in the profile of the epoxy matrix are observed, demonstrating that the fillers do not cause its chemical alteration. On the other hand, vibrational bands related to CB, APP and Si-Ti-Mg mixed oxide cannot be distinguished clearly, as they overlap with some of the epoxy bands.

3.2. *Flammability behavior of the hybrid epoxy nanocomposites*

To screen the flammability of pristine resin and epoxy nanocomposites, UL 94 vertical flame spread tests were performed on all the prepared formulations listed in Table S2. ESiTAC1P could be classified as V-0, due to its no dripping self-extinguishing behavior, while

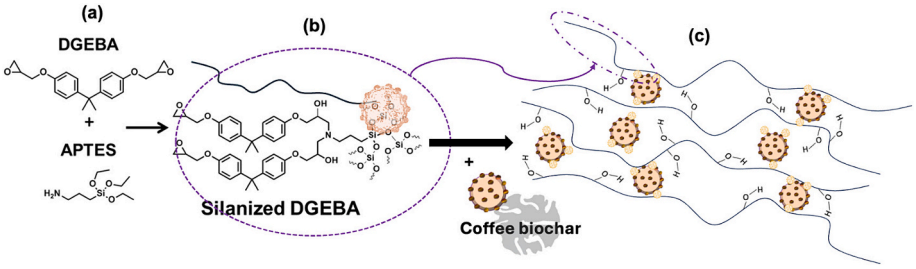

Scheme 2. Scheme of the formation of the hybrid epoxy network: DGEBA and APTES react to form silanized epoxy chains (a); hydrolysis and condensation reactions give rise to silica nanostructures (b); interactions between the hybrid polymer chains and the filler particles take place in the network (c).

ESiTAC0.5P was found to be V-1 rated, as the sample captures the flame, but it gives low values of after-flame times (Table S2). Concerning the other formulations, the flame reaches the holding clamp, completely burning the material, and thus none of these systems could be classified. However, in the case of ETA1P and ESiTA1P, t_1 extinguishing times could be collected (Table S2), revealing that the combined use of Si-Ti-Mg and APP, especially in the presence of a hybrid silica-epoxy phase (ESiTA1P), impacts on the charring process from the early combustion stages, lowering the flammability of epoxy resin. The weak acidic characteristics of Si-Ti-Mg and silanized epoxy chains, together with the acid phosphorus compounds released by APP during its decomposition, promote the dehydration of the polymer matrix, causing the formation of a protective, abundant, and continuous char [52]. Apart from E, all the other samples do not show any dripping during the test (Table S2), which additionally confirms the char-forming character of APTES-modified epoxy network, Si-Ti-Mg, CB, and APP. Taking into consideration the after-flame times of ETA1P, ESiTA1P, and ESiTAC1P, it is evident that the use of CB is crucial to achieving the V-0 rating. The hybrid silica-epoxy sample (ESiTAC1P) containing the highest amount of coffee biochar shows a limited burning and gives rise to the formation of a very coherent char, also due to a significant increase in the melt viscosity of the burning system. The use of an APTES-modified polymer network, a CB loading of ~20 wt%, and a concentration of phosphorus equal to 1 wt% were fundamental to obtain an epoxy system showing no dripping V-0 rating. Unlike ESiTAC0.5P and ESiTAC1P, ETAC1P and ESiTA1P could not be classified; this suggests a combined condensed phase action played by coffee biochar and the hybrid epoxy moieties (ESiTAC0.5P and ESiTAC1P samples), especially reducing the t_2 extinguishing time, probably ascribed to the production of an effective ceramic char acting as an oxygen barrier and thermal shield for the underlying polymer (Table S2) [22].

Based on the flammability results, in the following sections, only the outcomes resulting from the investigation of the thermal properties, mechanical performances, and fire behavior of UL 94 classifiable samples (i.e., ESiTAC0.5P and ESiTAC1P) and their unfilled counterparts (namely, E and ESi) will be discussed. In addition to these epoxy formulations, the fire parameters (see section 3.4) of ESiC will be also evaluated to study the influence of biochar on the flame retardant

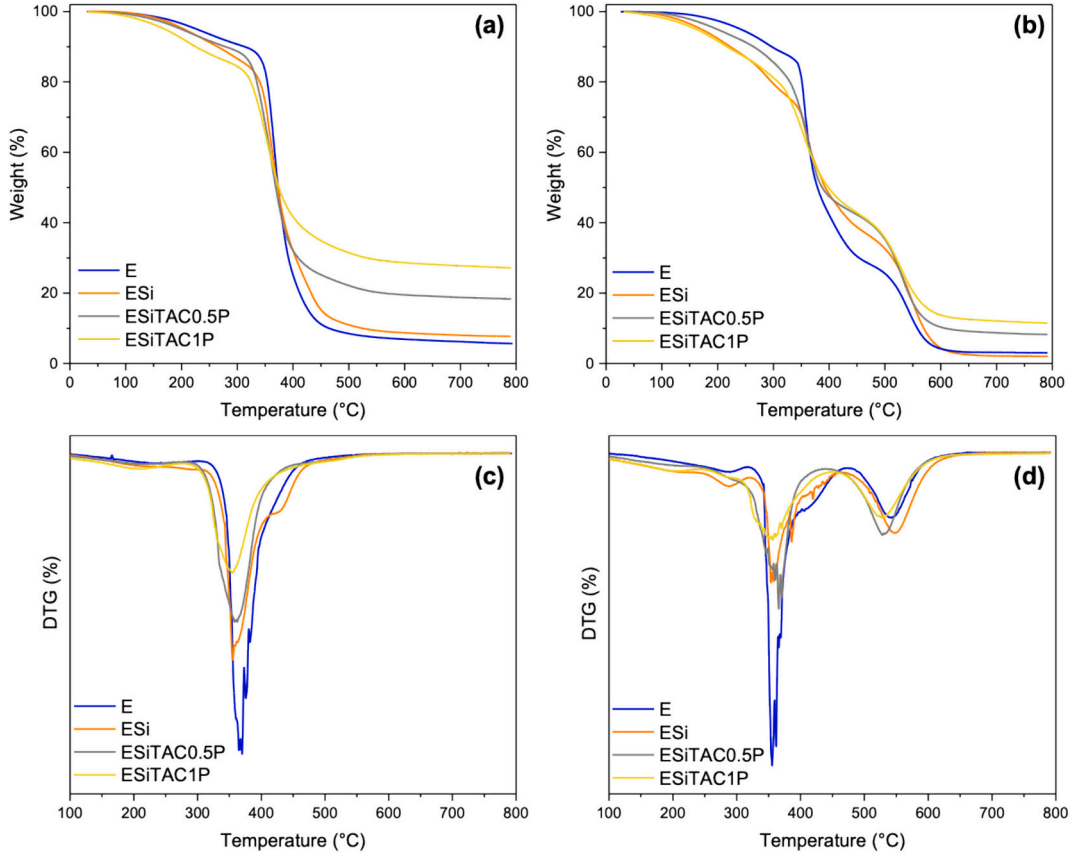

Fig. 2. TGA curves (a, b) and DTG curves (c, d) of pristine resin, silicon-modified epoxy resin, and epoxy nanocomposites under N_2 (a, c) and air (b, d).

features of ESi. LOI measurements were carried out on the above-selected samples to evaluate the minimum percentage of oxygen needed in an O_2/N_2 mixture to support the candle-like combustion after ignition. Table S3 shows that the concurrent presence of the hybrid silica-epoxy phase and CB (ESiC sample) slows down the candle-like combustion. However, the highest value of LOI is observed for ESiTAC1P, proving that the incorporation of Si-Ti-Mg, CB, and APP into the APTES-modified DGEBA polymer matrix is effective in enhancing the flame retardant behavior (Table S3). These results are in good agreement with the outcomes of the UL 94 vertical flame spread tests.

3.3. Thermal behavior of hybrid epoxy nanocomposites

Fig. 2a and c show the thermal decomposition profile of pristine resin and epoxy nanocomposites in nitrogen atmosphere. In agreement with similar aliphatic epoxy systems reported in the literature [53], all the samples display a main decomposition step at around 350 °C. The earlier mass loss (see $T_{5\%}$ in Table 2) in ESi can be ascribed to the acidic characteristics of hybrid silica-epoxy moieties, which favor the carbonization process via dehydration of epoxy resin [16]. This anticipation becomes even more evident in the case of ESiTAC0.5P and ESiTAC1P, where the presence of acidic phosphorus compounds, produced together with non-flammable volatiles (i.e., N_2 and phosphorous species) from the decomposition of APP, and acidic functionalities (see section 3.1) on the surface of coffee biochar and Si-Ti-Mg oxide boost the formation of an abundant pyrolytic char, leading to higher residual masses at 800 °C compared to E and ESi (Fig. 2a and Table 2). Fig. 2b and d report the thermogravimetric data in air. Here, it is possible to observe that the thermo-oxidative stability of ESi is strongly affected by the addition of APP, coffee biochar, and Si-Ti-Mg oxide, which allows for a notable increase in the residual mass at 800 °C (Table 2), especially when the amount of fillers and phosphorus increases (ESiTAC1P sample).

The better overall thermal stability of ESiTAC0.5P and ESiTAC1P may be due not only to the char-forming character of hybrid moieties and fillers but also to different mechanisms taking place during their degradation at high temperatures, namely: (i) the decomposition of APP in air, which produces nitrogen able to disrupt the diffusion of oxygen, (ii) the higher graphitization degree of the char formed in presence of CB (see Section 3.4), which limits the heat exchange at the boundary phase between the gas phase and the polymer bulk [37,54], and (iii) the degradation of the hybrid silica-epoxy network and the refractive chemical nature of Si-Ti-Mg oxide, which promote the formation of a stable aromatic char acting as effective thermal shield and barrier, also preventing the diffusion of decomposed gas and oxygen from the surroundings into the material.

Fig. S7 shows the typical DSC curves of pristine resin and hybrid epoxy composites. The absence of an exothermic peak in the first heating ramp, along the measured temperature range, confirms the completeness of the curing process for all the examined samples in the adopted experimental conditions. These results well agree with FTIR analyses.

The viscoelastic behavior of E and hybrid epoxy composites as a function of temperature was investigated using dynamic mechanical analysis. The maximum of tan δ curves (Fig. 3a) was evaluated to determine the glass transition temperatures of samples. Fig. 3a highlights the completely different behavior of E compared to hybrid materials, as its tan δ curve appears symmetric and narrow with the highest tan δ peak (at 96 °C); conversely, the other samples exhibit asymmetric and wider tan δ curves. Unlike the epoxy composites, E can easily dissipate the application of a load through energy dissipation mechanisms (e.g., segmental motions), though a part of the load is stored in the material and released only after the removal of the load. As observed in previous works [16,22], the different shape of tan δ curves related to ESi, ESiTAC0.5P, and ESiTAC1P is ascribed to a broad distribution of relaxation phenomena. In particular, the tan δ curve of ESi reveals the presence of two co-continuous phases with different chain mobilities in its polymer network [51]. In ESi, the hydrolysis of APTES-modified DGEBA polymer chains leads to the generation of a hybrid silica-epoxy phase bearing silanol groups able to establish hydrogen bonds with hydroxyl groups formed during the cross-linking process (Fig. 3c and d) [55]. These interactions lead to a second glass transition temperature, which is higher than that of E, and thus ESi shows a tan δ curve with two well-resolved maxima ($Tg_1 = 73$ °C, $Tg_2 = 105$ °C). The lower glass transition temperature is probably due to the presence of dangling segments causing a network loosening effect, as the APTES-modified epoxy chains cannot react with the hardener to form cross-linking points [56]. In the case of ESiTAC0.5P and ESiTAC1P, the presence of biochar and other additives negatively affects the occurrence of hydrogen bonds linked to the hybrid silica-epoxy phase, which is mainly responsible for the better dispersion of the coffee waste, resulting in the disappearance of the shoulder at higher temperature in their tan δ curves (Figs. 3a). ESiTAC0.5P and ESiTAC1P exhibit lower glass transition temperatures (82 °C and 79 °C, respectively) than E, probably due to the presence of biochar and other fillers that affect the inter-chain interactions during the cross-linking of the polymer matrix [57,58]. These phenomena become more relevant for ESiTAC1P, owing to the higher amount of fillers than ESiTAC0.5P. However, ESiTAC0.5P and ESiTAC1P show a maximum of tan δ at higher temperatures than ESi, as the additives, especially the biochar, can form a huge number of hydrogen bonds with the hydroxyl groups of cured epoxy chains (Fig. 3e and f), reducing the detrimental effect of dangling segments on the glass transition temperature and the mobility of the epoxy segments as well [27]. On the other side, the higher concentration of fillers in ESiTAC1P causes a hindering effect in the regular packing of the epoxy chains, leading to a slight decrease in the Tg value compared to that of ESiTAC0.5P (Fig. 3a and f). Given the above results, it appears clear that, compared to E, the hybrid epoxy composites exhibit a higher elastic response and a lower

Table 2
TGA analysis of all samples in air and N_2. $T_{5\%}$ is the temperature, at which 5 wt% loss occurs. T_{max1} and T_{max2} are the temperatures, at which the weight loss rate reaches a maximum; the residues at T_{max1}, T_{max2}, and 800 °C are also reported.

Sample	$T_{5\%}$ (°C)	$T_{10\%}$ (°C)	T_{max1} (°C)	T_{max2} (°C)	Residue (wt%) at		
					T_{max1}	T_{max2}	800 °C
Nitrogen							
E	227	312	367	–	60	–	5
ESi	204	264	359	–	64	–	7
ESiTAC0.5P	199	279	360	–	58	–	18
ESiTAC1P	170	225	356	–	61	–	27
Air							
E	241	294	358	544	69	12	3
ESi	170	220	355	548	67	23	2
ESiTAC0.5P	198	264	372	530	59	24	8
ESiTAC1P	161	218	357	529	64	27	11

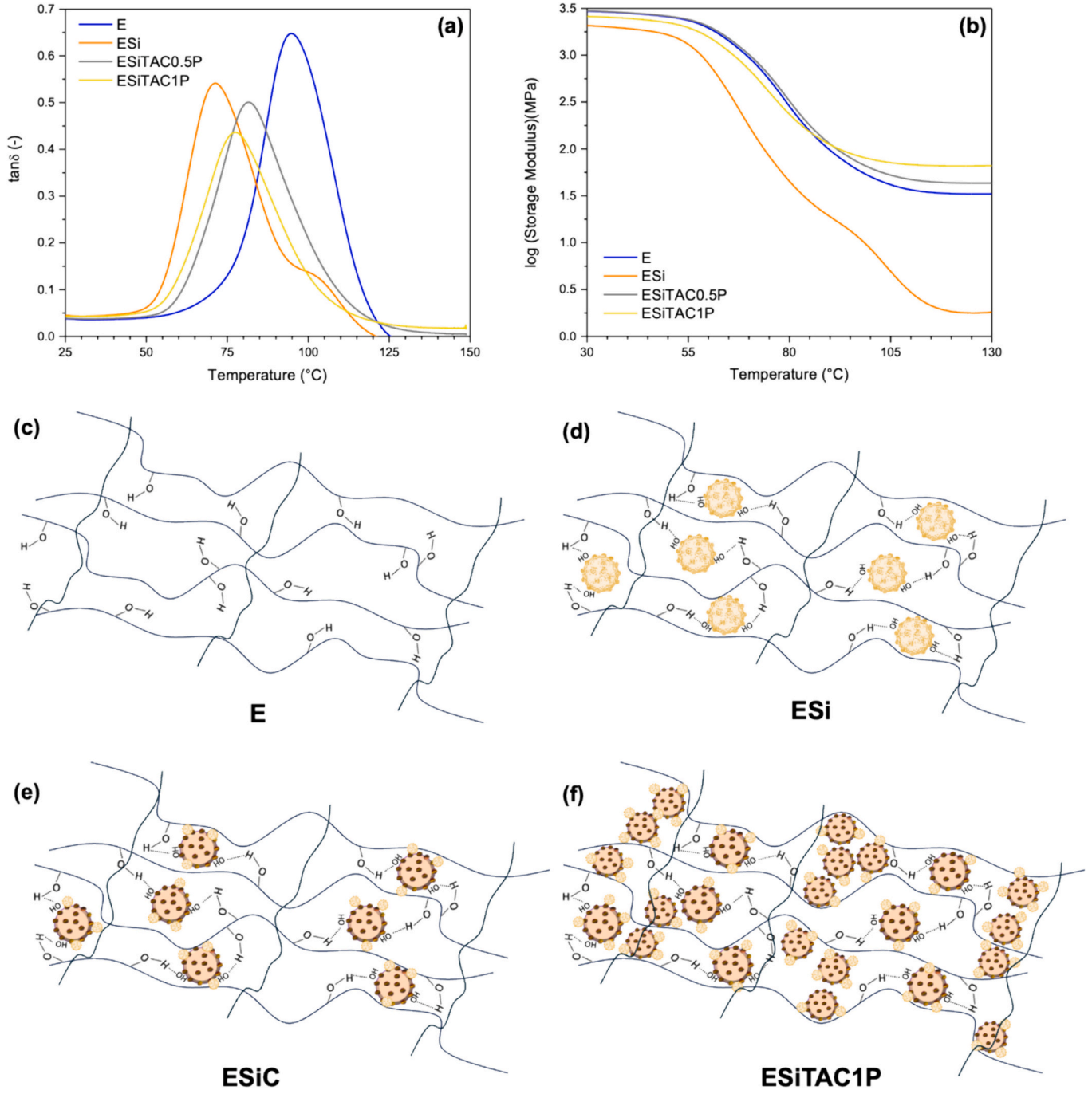

Fig. 3. Mechanical damping factor (tan δ) (a) and storage moduli (E′) (b) of pristine resin, silicon-modified epoxy resin, and epoxy nanocomposites, collected as a function of temperature. Scheme of cross-linked unmodified epoxy network (c) and possible hydrogen bonding interactions established between hydroxyls of cured epoxy resin, coffee biochar particles, and silanol groups in the hybrid epoxy nanocomposites (d, e, and f).

ability to dissipate the energy received from a load application. This elastic response is especially evident in ESi, where the presence of dangling segments, responsible for a predominant network loosening effect, leads to the lowest values of storage moduli (E') in the glassy state region (Fig. 3b), compared to the other composites [59]. On the contrary, the formation of several hydrogen bonds in ESiTAC0.5P and ESiTAC1P causes a predominant stiffening effect, resulting in E' values that approach those of E, even though the simultaneous hindering phenomena take place (Fig. 3b). Considering that the modification of the DGEBA epoxy matrix by APTES is crucial to obtain a uniform dispersion of coffee waste, the DMA characterization demonstrates that the incorporation of biochar, ternary metal oxide, and APP into the hybrid polymer system leads to a beneficial effect on the dynamic-mechanic behavior and mechanical properties of the final composites.

3.4. Fire behavior of hybrid epoxy nanocomposites

PCFC and cone calorimetry tests can shed light on the fire behavior of pristine resin and epoxy nanocomposites, allowing for a critical assessment of thermal and smoke parameters. CC tests are performed in air atmosphere and flammable gases, released by the application of an irradiative heat flux on the sample, undergo ignition using a spark. Conversely, PCFC is a nonflaming test, in which the material is pyrolyzed in an inert gas stream and then the evolved gaseous products are

separately oxidated [60,61]. PCFC and cone calorimetry are employed to deeply investigate the flame retardant mechanisms occurring during the combustion of flame retarded systems. PCFC results are collected in Table S4, while the related heat release rate (HRR) curves as a function of temperature are displayed in Fig. 4. Compared to E, ESi and epoxy nanocomposites exhibit decreased heat release capacity (HRC), pHRR, and total heat release (THR) values (Table S4), suggesting that hybrid moieties and additives (APP, CB, and Si-Ti-Mg oxide) can slow down the pyrolysis of the polymer network and the release of flammable gases. PCFC outcomes also highlight that CB acts as a strong char-promoter, as its incorporation into ESi causes a remarkable decrease (~23%) in pHRR as well as a notable increase (4.3 wt%) in the residue at the end of the test (Table S4). On the other side, the combined use of CB, Si-Ti-Mg, and APP (ESiTAC1P) does not lead to an additional increase in the residual mass. However, the presence of the P-based flame retardant in ESiTAC1P significantly lowers the pHRR value (Fig. 4a, Table S4), likely due to a slight depletion of oxygen by the action of phosphorus species in the oxidation chamber.

The fire performances of virgin resin and epoxy nanocomposites were further studied by cone calorimetry tests. Fig. 4b and Table 3 show that the presence of the hybrid silica phase alone allows for a significant reduction (32%) in pHRR compared to pristine resin. This finding supports the boosting effect of silica-epoxy moieties in the formation of a silicon-containing ceramic char acting as a thermal barrier during the combustion, as can be observed in the Raman spectra reported in Fig. 5.

As shown in Fig. 5, char recovered from E shows the signal of highly carbonized material with a well-defined G peak and a small D peak. The addition of APTES significantly changes the Raman pattern with very intense peaks due to $\nu_{O\text{-}H}$ of silicon residues, while the presence of CB witnesses the structuring of the D/G peak region. The complexity of both ESiTAC0.5P and ESiTAC1P can be appreciated by the signal at low Raman shift linked to the M–O bonds.

As shown in Fig. S8a, the char formed after the combustion of E looks like a carbon soot with quasi-spherical nanometric particles of average diameter around 20–30 nm, while the one resulting from the decomposition of ESi appears more continuous due to the increment (up to 50 nm) in average diameter and thus it is capable of acting as a more effective barrier toward the diffusion of oxygen and flammable gases [56]. Cone calorimetry results confirm the dehydrating effect and char-forming behavior of APTES-modified epoxy network, Si-Ti-Mg oxide, CB, and APP, as all the formulations promote lower values of Time To Ignition (TTI) and higher residual masses, compared with the unfilled resin (Table 3). This finding well agrees with the decrease in CO/CO_2 ratio observed for all the epoxy nanocomposites but E, highlighting a predominant condensed phase action exerted by the hybrid epoxy moieties and functional additives in the flame retardation of the epoxy matrix, which well agrees with the results of PCFC measurements (Tables 3 and S4) [56]. ESiC exhibits a pHRR value that is 65% lower than that of E (Table 3), showing that the addition of CB into the APTES-modified epoxy network appears crucial to significantly improve the fire behavior of the epoxy system [62]. Also, the broadening of the heat release rate curve of ESiC reveals a slow heat release over a longer timespan compared to that of blank epoxy (Fig. 4b). Fig. S8c displays that the combustion of ESiC provides a char with a morphology close to the one of the carbonaceous residue resulting from the decomposition of ESi, but less abundant in carbon soot-like particles. However, CB particles can act as sites for the formation of silicon-based layered carbon hybrid structures, whose chemical composition still shows a notable Si retention (Table S5). Overall, the char resulting from ESiC exhibits a significantly higher amount of carbon up to 82.6 wt% than the one produced from the combustion of ESi (74.5 wt%), as reported in Table S5. The presence of silicon-based layered carbon hybrid structures

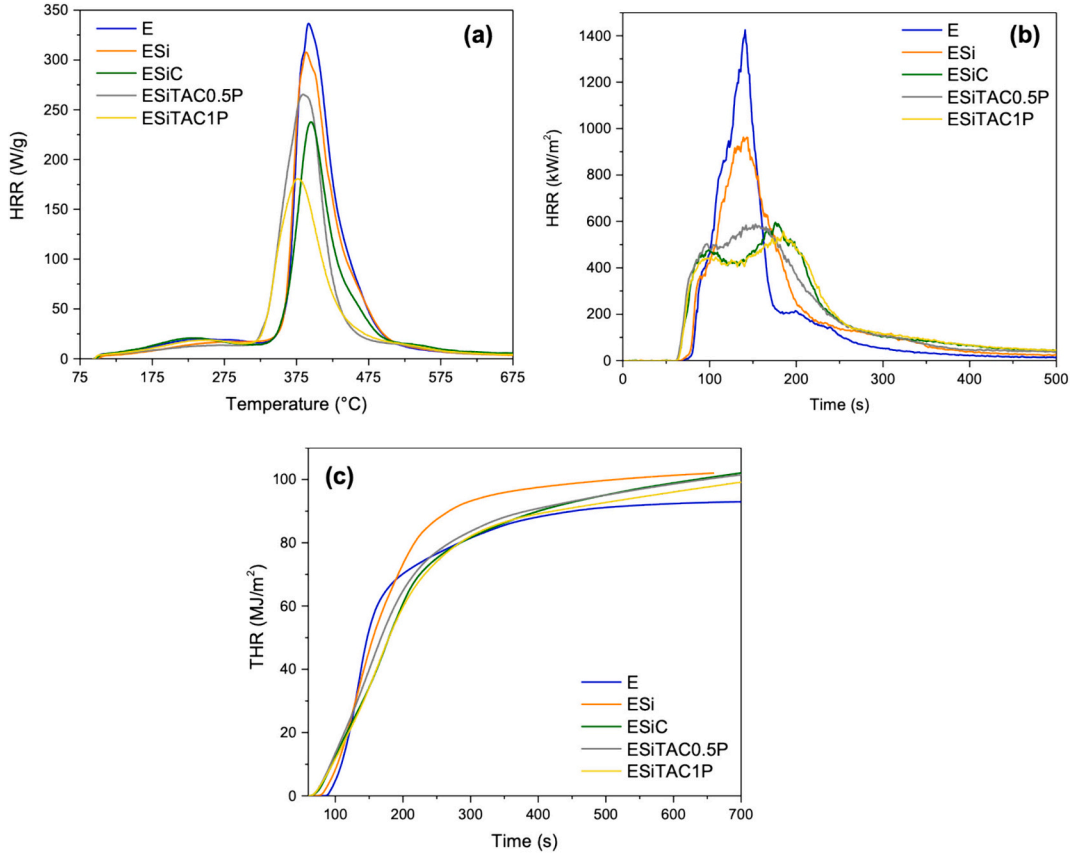

Fig. 4. Heat release rate curves of pristine resin, silicon-modified epoxy resin, and epoxy nanocomposites measured by pyrolysis flow combustion calorimetry (a) and cone calorimetry (CC) tests (b). The total heat release curves (c) for the same samples determined by CC tests are also reported.

Table 3
Results from cone calorimetry tests for the investigated epoxy samples.

Sample	TTI (s)	TTFO (s)	THR (MJ/m^2)	HRR (kW/m^2)	pHRR (kW/m^2)	ΔpHRR (%)	FRI (–)	Residue (wt%)
E	26 ± 1	593 ± 14	93 ± 4	467 ± 12	1424 ± 68	–	–	3 ± 0.5
ESi	22 ± 1	549 ± 97	99 ± 2	432 ± 11	962 ± 65	−32	1.1	4 ± 0.3
ESiC	15 ± 2	570 ± 37	99 ± 3	346 ± 9	491 ± 73	−65	1.5	17 ± 0.7
ESiTAC0.5P	11 ± 0	479 ± 53	102 ± 4	378 ± 2	588 ± 31	−58	0.9	9 ± 0.5
ESiTAC1P	14 ± 2	527 ± 86	103 ± 2	355 ± 2	557 ± 14	−61	1.2	18 ± 0.3

TTI = Time To Ignition, **TTFO** = Time To Flame Out, **THR** = Total Heat Release, **HRR** = Heat Release Rate, **pHRR** = peak of Heat Release Rate, **FRI** = Flame Retardancy Index.

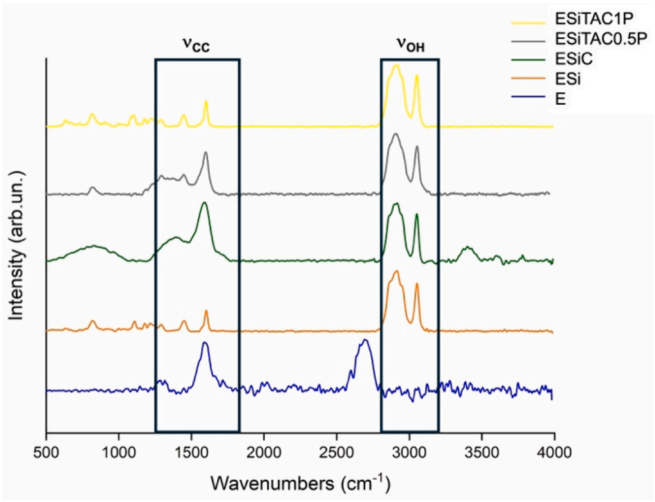

Fig. 5. Raman spectra of char recovered after UL 94 vertical flame spread tests.

boosts the flame retardant action of CB in the condensed phase, mainly reducing the pHRR and the heat exchange at the boundary phase over time (Table 3) [39,63].

The incorporation into ESi of CB alone (ESiC) or in combination with APP and Si-Ti-Mg oxide (ESiTAC0.5P and ESiTAC1P) slows down the heat release rate (Fig. 4c) and extends the time to pHRR (Fig. 4b and Table 3), probably due to the condensed phase action of biochar particles, ternary oxide species, and acidic phosphorus compounds. The degradation of APP causes the production of nitrogen able to act as a diluting agent in the gas phase during burning: this may explain the slightly higher TTI of ESiTAC1P compared to ESiTAC0.5P (Table 3 and Fig. 4b). The effect of APP on the values of TTI and residual char, together with its capability to release phosphorous radicals, poisoning oxygen radicals in the flame [64], may explain the self-extinguishing and better fire behavior of ESiTAC1P with respect to ESiTAC0.5P, in which the overall fillers' loading is lower. However, the good fire behavior of ESiTAC1P may be mainly ascribed to the formation of a complex protective char with a low amount of carbon soot-like particles and numerous layered inorganic carbon hybrid structures (Figs. S8 d and e). Furthermore, the char formed by the combustion of ESiTAC1P appears significantly more graphitic compared to the one of ESiC, as shown in Fig. 5, in which well resolved small D and G peaks can be observed. Similarly to the one obtained from the decomposition of ESiC, this char still has a silicon retention up to 0.9 wt%. The FRI is an extensively used dimensionless parameter (see section 2.4), which allows for comparing the fire behavior of flame retardant polymer-based composites with the one of their unfilled counterparts and rank a specific material based on its fire response [65]. The FRI value of ESiTAC1P was found to be basically the same of other systems containing similar amounts of APP (Table 3) [36,37]. ESiC and ESiTAC1P exhibit the highest FRI values, settling at around a "good" classification, which additionally confirms the crucial role of CB in enhancing the fire performances of the polymer matrix. These results agree with what was observed for epoxy nanocomposites, where the in-situ generation of inorganic phases contributed to the condensed phase action in synergy with the main flame retardant component [13,66].

Given the above results, a simplified flame retardant mechanism is proposed (Fig. 6a), which illustrates the different phenomena taking place during the combustion of all the prepared formulations.

More in detail, as already observed in previous epoxy systems with similar chemical composition [67], the combustion of ESiTAC1P may lead to the generation of P–N–O–Si–O–P polymeric substructures on the surface able to boost the thermal shielding action of the carbonaceous material during the combustion. The generation of P–N–O–Si–O–P polymeric substructures is due to the condensation between silanol groups of the hybrid epoxy network and P–N–O substructures, which are formed by the reaction between ammonia and acid phosphorous compounds, both derived from the decomposition of APP at around 250 °C. P–N–O–Si–O–P polymeric substructures are responsible for the stretching vibrations of P-C and P-O groups present in the FTIR spectrum of residual char formed by ESiTAC1P (Fig. 6b) [22]. Further, this spectrum shows a broad band related to Ti-O bonds arising from the presence of Si-Ti-Mg in ESiTAC1P, which is also accountable for the appearance of magnesium in the EDX analysis of the char as shown in Table S5. The use of Si-Ti-Mg not only promotes the charring of the polymer matrix but also contributes to the formation of a ceramic protective char during the combustion of ESiTAC1P (Fig. 6a), which additionally lowers the heat exchange at the boundary phase. The strong band at 1577 cm^{-1} related to the C═C stretching vibration, clearly visible in the FTIR spectrum of ESiTAC1P (Fig. 6b), highlights significant carbonization via dehydration of the epoxy resin promoted by hybrid silanized chains, CB, Si-Ti-Mg oxide, and acidic phosphorus compounds [68,69]. On the other side, the peaks at 638 cm^{-1}, 802 cm^{-1}, and 871 cm^{-1} are ascribed to aromatic C-H out-of-plane vibrations in meta, para, and ortho, respectively [61,70]. The presence of these peaks proves that this char contains more aromatic structures compared to that of both pristine resin and ESi.

It is worth noting that the incorporation of CB into the hybrid silanized epoxy guarantees the lowest value of TSP and causes a significant flattening of the SPR curve compared to E (Table 4 and Fig. S9a). The incorporation of CB alone or in combination with Si-Ti-Mg oxide into ESi leads to a slow smoke production over a longer timespan especially compared to that of pristine epoxy (Fig. S9b) [71]. Despite their flame retardant action, CB and Si-Ti-Mg oxide do not increase the total smoke production (Table 4 and Fig. S9a), probably due to the ability of porous biochar (Fig. 1) to adsorb gases (e.g., phenol, cresol, carbon dioxide, naphthalene, anthracene, among others) and the basic characteristics of magnesium oxide in the ternary system (Figs. 6a and Table S5), which limits the emission of acid compounds composing the smoke flow [72].

3.5. Mechanical behavior of hybrid epoxy nanocomposites

To further support DMA results (section 3.3) and shed some light on the mechanical performances of E, ESi, ESiTAC0.5P, and ESiTAC1P, the flexural behavior of these samples was studied (Table 5). ESi shows the lowest value of modulus (E_B) compared to the pristine resin and the

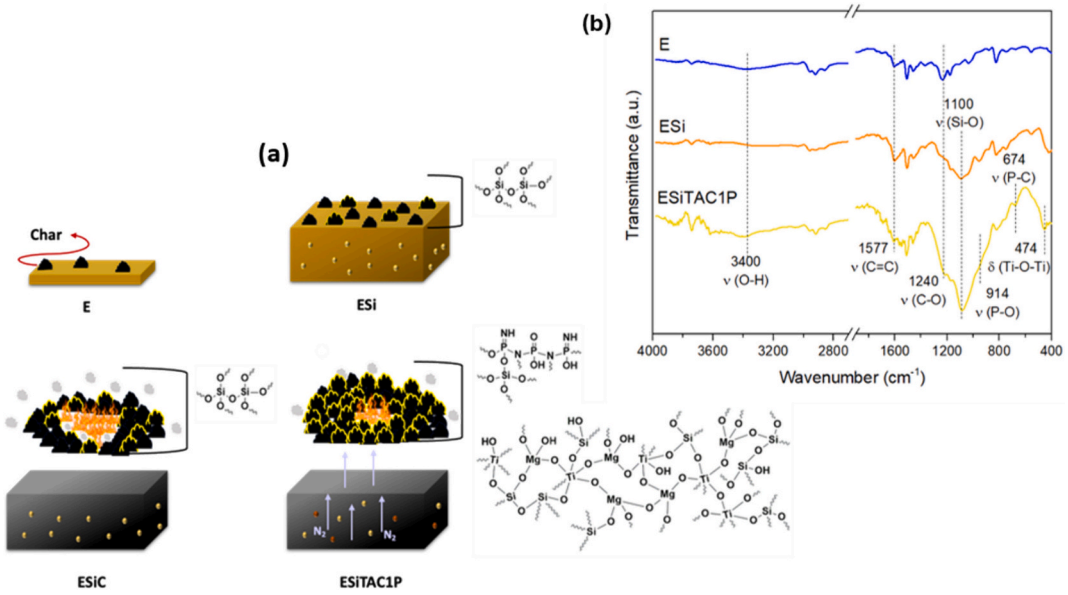

Fig. 6. Proposed mechanisms of ammonium polyphosphate, coffee biochar particles, and metal ternary (Si-Ti-Mg) oxide in the flame retardation of the silicon-modified epoxy resin (a). The yellow balls represent the silicon-modified epoxy chains, while the red ones indicate the Si-Ti-Mg oxide particles. On the right, (b) FTIR spectra of residual chars after UL 94 vertical flame spread tests carried out on pristine resin, silicon-modified epoxy resin, and epoxy nanocomposites.

Table 4
Smoke parameters from cone calorimetry tests for the studied epoxy samples.

Sample	TSP (m^2)	SEA (m^2/kg)	CO/CO_2 (–)
E	27 ± 1.0	797 ± 37	0.33
ESi	28 ± 1.0	813 ± 26	0.25
ESiC	24 ± 0.8	728 ± 11	0.22
ESiTAC0.5P	26 ± 0.6	788 ± 13	0.22
ESiTAC1P	25 ± 0.3	769 ± 0.5	0.20

TSP = Total Smoke Production, **SEA** = Specific Extension Area.

Table 5
Flexural test results of pure epoxy resin, silicon-modified epoxy resin, and epoxy nanocomposites for comparison.

Sample	E_B (MPa)	$\sigma_{u,B}$ (MPa)	$\varepsilon_{f,B}$ (%)
E	3231 ± 468	138 ± 3	6.5 ± 0.9
ESi	2743 ± 14	107 ± 15	5.5 ± 0.1
ESiTAC0.5P	3622 ± 311	45 ± 5	1.4 ± 0.3
ESiTAC1P	3713 ± 88	49 ± 2	1.5 ± 0.1

other hybrid composites, probably due to its looser network characterized by segments of longer APTES-modified epoxy chains, which account for higher values of fracture strength ($\sigma_{u,B}$) and elongation at break ($\varepsilon_{f,B}$) (Table 5). With respect to E and ESi, epoxy formulations containing biochar and other fillers, ESiTAC0.5P and ESiTAC1P, exhibit higher E_B but lower $\sigma_{u,B}$ and $\varepsilon_{f,B}$ values (Table 5), attributable to the hydrogen bonding interactions and the steric hindrance of the fillers. The presence of Si-Ti-Mg, CB, and APP in the APTES-modified DGEBA polymer matrix causes a decrease in the motion of the chain segments leading to topological constraints and stiffer networks [51]. These results well agree with previous works reported in the literature, as inorganic particles of flame retardants or other additives are generally responsible for making polymer-based matrices less ductile and more brittle [73–75].

4. Conclusions

Spent coffee grounds represent one of the most abundant wastes in the world. The pyrolysis of this waste allows to produce biochar suitable for providing epoxy resins with enhanced features. In this work, we investigated the intriguing and unprecedented use of coffee biochar as a flame retardant component in silicon-modified epoxy resin. The sol-gel modification of the polymer matrix accounted for the excellent distribution of CB within the resin. Cone calorimetry tests revealed that the incorporation of CB into the silicon-modified DGEBA resin favors the formation of an abundant ceramic char, resulting in a significant decrease (~65%) in the peak heat release rate compared with the pristine resin. The use of 20 wt% CB, together with APP and a ternary mixed oxide (Si-Ti-Mg), was crucial to obtain no dripping self-extinguishing (UL 94-V-0 rating) hybrid epoxy nanocomposites with only 1 wt% of phosphorus loading. However, flammability tests prove that the presence of CB was required to tip the balance in favor of low extinguishing times after flame application. Cone calorimetry, pyrolysis flow combustion calorimetry, and mechanical tests revealed that the addition of CB, APP, and Si-Ti-Mg oxide to the hybrid epoxy system leads to a strong reduction (up to 42%) in pHRR values, a longer time to peak of heat release rate, and a notable increase (up to 35%) in flexural modulus, respectively. Besides, microscopy analysis and Raman spectroscopy of residual chars confirm that CB plays a key role in the flame retardation of the silicon-modified epoxy resin, as it contributes with APP and Si-Ti-Mg oxide to the formation of a highly graphitized continuous char containing N–P–O–Si substructures, acting as a thermal shield and oxygen barrier in the condensed phase during the decomposition of the epoxy matrix. CO/CO_2 ratios measured during CC tests additionally supported a predominant flame retardant action in the condensed phase exerted by CB and the other fillers.

In conclusion, we demonstrated that the generation of silicon-modified hybrid epoxy moieties enables the uniform distribution of CB, which can be effectively employed, in combination with other additives, as a green flame retardant for the manufacturing of thermosets with improved fire behavior and satisfactory mechanical properties. The proposed strategy may be of inspiration to foster the development of more self-extinguishing aliphatic epoxy products, using sustainable fillers (e.g., various types of biochars), low concentrations of phosphorus, and bio-based polymer matrices.

CRediT authorship contribution statement

Aurelio Bifulco: Writing – original draft, Validation, Methodology, Investigation, Formal analysis, Conceptualization. **Mattia Bartoli:** Writing – original draft, Investigation, Formal analysis. **Immacolata Climaco:** Visualization, Investigation, Formal analysis. **Maria Cristina Franchino:** Visualization, Investigation. **Daniele Battegazzore:** Investigation, Formal analysis. **Rhoda Afriyie Mensah:** Investigation, Formal analysis. **Oisik Das:** Visualization, Investigation, Formal analysis. **Henri Vahabi:** Writing – review & editing, Methodology, Conceptualization. **Giulio Malucelli:** Writing – review & editing, Validation, Supervision, Methodology, Conceptualization. **Antonio Aronne:** Writing – review & editing, Validation, Supervision, Resources. **Claudio Imparato:** Writing – original draft, Validation, Investigation, Formal analysis, Conceptualization.

Declaration of competing interest

Aurelio Bifulco reports financial support was provided by the Italian Ministry of Education and Research. Aurelio Bifulco reports a relationship with the University of Naples Federico II that includes: employment. The other authors declare that they have no known competing financial interests or personal relationships that could have appeared to influence the work reported in this paper.

Data availability

Data will be made available on request.

Acknowledgements

Dr. Aurelio Bifulco acknowledges the Italian Ministry of Education and Research, PON R&I 2014-2020 – Asse IV "Istruzione e ricerca per il recupero – REACT-EU" – Azione IV.6 – "Contratti di ricerca su tematiche Green", for the financial support concerning his employment contract.

Appendix A. Supplementary data

Supplementary data to this article can be found online at https://doi.org/10.1016/j.susmat.2024.e01079.

References

[1] W. He, P. Song, B. Yu, Z. Fang, H. Wang, Flame retardant polymeric nanocomposites through the combination of nanomaterials and conventional flame retardants, Prog. Mater. Sci. 114 (2020) 100687, https://doi.org/10.1016/j.pmatsci.2020.100687.

[2] P. Wiśniewska, N.A. Wójcik, J. Ryl, R. Bogdanowicz, H. Vahabi, K. Formela, M. R. Saeb, Rubber wastes recycling for developing advanced polymer composites: a warm handshake with sustainability, J. Clean. Prod. 427 (2023) 139010, https://doi.org/10.1016/j.jclepro.2023.139010.

[3] G. Martínez-Narro, S. Hassan, A.N. Phan, Chemical recycling of plastic waste for sustainable polymer manufacturing – a critical review, J. Environ. Chem. Eng. 12 (2024) 112323, https://doi.org/10.1016/j.jece.2024.112323.

[4] G.R. Mong, H. Tan, D.D.C.V. Sheng, H.Y. Kek, B.B. Nyakuma, K.S. Woon, M.H. D. Othman, H.S. Kang, P.S. Goh, K.Y. Wong, A review on plastic waste valorisation to advanced materials: solutions and technologies to curb plastic waste pollution, J. Clean. Prod. (2023) 140180, https://doi.org/10.1016/j.jclepro.2023.140180.

[5] B. Liu, H. Zhao, Y. Wang, Advanced flame-retardant methods for polymeric materials, Adv. Mater. 34 (2022) 2107905, https://doi.org/10.1002/adma.202107905.

[6] G. Ye, S. Huo, C. Wang, Q. Zhang, B. Wang, Z. Guo, H. Wang, Z. Liu, Fabrication of flame-retardant, strong, and tough epoxy resins by solvent-free polymerization with bioderived, reactive flame retardant, Sustain. Mater. Technol. (2024) e00853, https://doi.org/10.1016/j.susmat.2024.e00853.

[7] Y.-R. Zhang, S. Gu, Y.-Z. Wang, L. Chen, Intrinsically flame-retardant epoxy vitrimers with catalyst-free multi-reprocessability towards sustainable carbon fiber composites, Sustain. Mater. Technol. 40 (2024) e00883, https://doi.org/10.1016/j.susmat.2024.e00883.

[8] J.C. Markwart, A. Battig, L. Zimmermann, M. Wagner, J. Fischer, B. Schartel, F. R. Wurm, Systematically Controlled Decomposition Mechanism in Phosphorus Flame Retardants by Precise Molecular Architecture: P–O vs P–N 1, 2019, pp. 1118–1125, https://doi.org/10.1021/acsapm.9b00129.

[9] J. Wang, J. Wang, S. Yang, X. Chen, K. Chen, G. Zhou, X. Liu, L. Xu, S. Huo, P. Song, H. Wang, Multifunctional phosphorus-containing imidazoliums endowing one-component epoxy resins with superior thermal latency, heat resistance, mechanical properties, and fire safety, Chem. Eng. J. 485 (2024) 149852, https://doi.org/10.1016/j.cej.2024.149852.

[10] Q. Yang, J. Wang, X. Chen, S. Yang, S. Huo, Q. Chen, P. Guo, X. Wang, F. Liu, W. Chen, P. Song, H. Wang, A phosphorus-containing tertiary amine hardener enabled flame retardant, heat resistant and mechanically strong yet tough epoxy resins, Chem. Eng. J. 468 (2023) 143811, https://doi.org/10.1016/j.cej.2023.143811.

[11] Y. Wang, L. Liu, L. Ma, J. Yuan, L. Wang, H. Wang, F. Xiao, Z. Zhu, Transparent, flame retardant, mechanically strengthened and low dielectric EP composites enabled by a reactive bio-based P/N flame retardant, Polym. Degrad. Stab. 204 (2022) 110106, https://doi.org/10.1016/j.polymdegradstab. 2022.110106.

[12] H. Fan, J. Zhao, J. Zhang, H. Li, S. Zhang, J. Sun, F. Xin, F. Liu, Z. Qin, W. Tang, TiO_2/SiO_2/kaolinite hybrid filler to improve the flame retardancy, smoke suppression and anti-aging characteristics of epoxy resin, Mater. Chem. Phys. 277 (2022) 125576, https://doi.org/10.1016/j.matchemphys.2021.125576.

[13] A. Bifulco, C. Imparato, A. Aronne, G. Malucelli, Flame retarded polymer systems based on the sol-gel approach: recent advances and future perspectives, J. Sol-Gel Sci. Technol. (2022) 1–25, https://doi.org/10.1007/s10971-022-05918-6.

[14] D. Battegazzore, M. Lavaselli, B. Cheng, D. Li, R. Yang, A. Frache, G. Paul, L. Marchese, Reactive extrusion of sol-gel silica as fire retardant synergistic additive in ethylene-vinyl acetate copolymer (EVA) composites, Polym. Degrad. Stab. 167 (2019) 259–268, https://doi.org/10.1016/j.polymdegradstab.2019.07.011.

[15] G. Camino, G. Tartaglione, A. Frache, C. Manferti, G. Costa, Thermal and combustion behaviour of layered silicate–epoxy nanocomposites, Polym. Degrad. Stab. 90 (2005) 354–362, https://doi.org/10.1016/j.polymdegradstab.2005.02.022.

[16] Z. Cheng, M. Fang, X. Chen, Y. Zhang, Y. Wang, H. Li, J. Qian, Thermal stability and flame Retardancy of a cured trifunctional epoxy resin with the synergistic effects of silicon/titanium, ACS Omega 5 (2020) 4200–4212, https://doi.org/10.1021/acsomega.9b04050.

[17] P. Li, L. Li, L. Ji, L. Dang, S. Lan, D. Zhu, Functionalized magnesium hydroxide with zinc borate and 3-aminopropyltriethoxysilane for enhanced flame retardant and smoke suppressant properties of epoxy resins, J. Appl. Polym. Sci. 140 (2023) e53941, https://doi.org/10.1002/app.53941.

[18] O. Das, N.K. Kim, M.S. Hedenqvist, D. Bhattacharyya, E. Johansson, Q. Xu, S. Holder, Naturally-occurring bromophenol to develop fire retardant gluten biopolymers, J. Clean. Prod. 243 (2020) 118552, https://doi.org/10.1016/j.jclepro.2019.118552.

[19] Y. Wang, J. Yuan, L. Ma, X. Yin, Z. Zhu, P. Song, Fabrication of anti-dripping and flame-retardant polylactide modified with chitosan derivative/aluminum hypophosphite, Carbohydr. Polym. 298 (2022) 120141, https://doi.org/10.1016/j.carbpol.2022.120141.

[20] X. Wang, G. Yang, H. Guo, Tannic acid as biobased flame retardants: a review, J. Anal. Appl. Pyrolysis (2023) 106111, https://doi.org/10.1016/j.jaap.2023.106111.

[21] B.K. Kandola, F. Magnoni, J.R. Ebdon, Flame retardants for epoxy resins: application-related challenges and solutions, J. Vinyl Addit. Technol. 28 (2022) 17–49, https://doi.org/10.1002/vnl.21890.

[22] V. Venezia, S. Matta, S. Lehner, G. Vitiello, A. Costantini, S. Gaan, G. Malucelli, F. Branda, G. Luciani, A. Bifulco, Detailed thermal, fire, and mechanical study of silicon-modified epoxy resin containing humic acid and other additives, ACS Appl. Polym. Mater. 3 (2021) 5969–5981, https://doi.org/10.1021/acsapm.1c01240.

[23] Y. Leow, P.Y.M. Yew, P.L. Chee, X.J. Loh, D. Kai, Recycling of spent coffee grounds for useful extracts and green composites, RSC Adv. 11 (2021) 2682–2692, https://doi.org/10.1039/d0ra09379c.

[24] A. Forcina, A. Petrillo, M. Travaglioni, S. di Chiara, F. De Felice, A comparative life cycle assessment of different spent coffee ground reuse strategies and a sensitivity analysis for verifying the environmental convenience based on the location of sites, J. Clean. Prod. 385 (2023) 135727, https://doi.org/10.1016/j.jclepro.2022.135727.

[25] G. Dattatraya Saratale, R. Bhosale, S. Shobana, J.R. Banu, A. Pugazhendhi, E. Mahmoud, R. Sirohi, S. Kant Bhatia, A.E. Atabani, V. Mulone, J.J. Yoon, H. Seung Shin, G. Kumar, A review on valorization of spent coffee grounds (SCG) towards biopolymers and biocatalysts production, Bioresour. Technol. 314 (2020) 123800, https://doi.org/10.1016/j.biortech.2020.123800.

[26] H. Vahabi, M. Jouyandeh, T. Parpaite, M.R. Saeb, S. Ramakrishna, Coffee wastes as sustainable flame retardants for polymer materials, Coatings 11 (2021) 1021, https://doi.org/10.3390/coatings11091021.

[27] W. Yang, W. Chang, J. Zhang, G.H. Yeoh, C. Boyer, C.H. Wang, Effects of waste coffee grounds on the mechanical properties, flame retardancy and toxic gas production of epoxy composites, Mater. Des. 224 (2022) 111347, https://doi.org/10.1016/j.matdes.2022.111347.

[28] M. Giorcelli, M. Bartoli, Development of coffee biochar filler for the production of electrical conductive reinforced plastic, Polymers (Basel). 11 (2019) 1916, https://doi.org/10.3390/polym11121916.

[29] A. Alhelal, Z. Mohammed, S. Jeelani, V.K. Rangari, 3D printing of spent coffee ground derived biochar reinforced epoxy composites, J. Compos. Mater. 55 (2021) 3651–3660, https://doi.org/10.1177/00219983211002237.

[30] L. Li, D. Zou, Z. Xiao, X. Zeng, L. Zhang, L. Jiang, A. Wang, D. Ge, G. Zhang, F. Liu, Biochar as a sorbent for emerging contaminants enables improvements in waste management and sustainable resource use, J. Clean. Prod. 210 (2019) 1324–1342, https://doi.org/10.1016/j.jclepro.2018.11.087.

[31] M. Bartoli, R. Arrigo, G. Malucelli, A. Tagliaferro, D. Duraccio, Recent advances in biochar polymer composites, Polymers (Basel). 14 (2022) 2506, https://doi.org/10.3390/polym14122506.

[32] T.A. Tengku Yasim-Anuar, L.N. Yee-Foong, A.A. Lawal, M.A. Ahmad Farid, M. Z. Mohd Yusuf, M.A. Hassan, H. Ariffin, Emerging application of biochar as a renewable and superior filler in polymer composites, RSC Adv. 12 (2022) 13938–13949, https://doi.org/10.1039/d2ra01897g.

[33] O. Das, D. Bhattacharyya, A.K. Sarmah, Sustainable eco-composites obtained from waste derived biochar: a consideration in performance properties, production costs, and environmental impact, J. Clean. Prod. 129 (2016) 159–168, https://doi.org/10.1016/j.jclepro.2016.04.088.

[34] J. Jiao, P. Liu, L. Wang, Y. Cai, One-step synthesis of improved silica/epoxy nanocomposites with inorganic-organic hybrid network, J. Polym. Res. 20 (2013) 1–8, https://doi.org/10.1007/s10965-013-0202-9.

[35] A. Tagliaferro, M. Rovere, E. Padovano, M. Bartoli, M. Giorcelli, Introducing the novel mixed gaussian-lorentzian lineshape in the analysis of the raman signal of biochar, Nanomaterials 10 (2020) 1748, https://doi.org/10.3390/nano10091748.

[36] W. Zhang, X. He, T. Song, Q. Jiao, R. Yang, The influence of the phosphorus-based flame retardant on the flame retardancy of the epoxy resins, Polym. Degrad. Stab. 109 (2014) 209–217, https://doi.org/10.1016/j.polymdegradstab. 2014.07.023.

[37] E. Movahedifar, H. Vahabi, M.R. Saeb, S. Thomas, Flame retardant epoxy composites on the road of innovation: an analysis with flame retardancy index for future development, Molecules 24 (2019) 3964, https://doi.org/10.3390/molecules24213964.

[38] F. Tuinstra, J.L. Koeing, Raman spectrum of graphite, J. Chem. Phys. 53 (1970) 1126–1130, https://doi.org/10.1063/1.1674108.

[39] X. Qiu, X. Wan, Z. Wang, Z. Li, J. Li, X. Li, Z. Zhang, A simple and universal strategy for construction and application of silica-based flame-retardant nanostructure, Compos. Part B Eng. 238 (2022) 109887, https://doi.org/10.1016/j.compositesb.2022.109887.

[40] M. Martins, C.M.C. Pereira, A study on the effect of nano-magnesium hydroxide on the flammability of epoxy resins, Solid State Phenom. 151 (2009) 72–78, https://doi.org/10.4028/www.scientific.net/SSP.151.72.

[41] X. Lv, H. Fan, W. Zeng, Z. Yang, Y. Wang, Z. Lei, Novel nanocomposites based on epoxy resin and modified magnesium hydroxide: focus on flame retardancy and mechanical properties, Polym. Adv. Technol. 30 (2019) 3026–3037, https://doi.org/10.1002/pat.4734.

[42] K.T. Ranjit, K.J. Klabunde, Solvent effects in the hydrolysis of magnesium methoxide, and the production of nanocrystalline magnesium hydroxide. An aid in understanding the formation of porous inorganic materials, Chem. Mater. 17 (2005) 65–73, https://doi.org/10.1021/cm040360b.

[43] H.S. Jung, J.-K. Lee, J.Y. Kim, K.S. Hong, Synthesis of nano-sized MgO particle and thin film from diethanolamine-stabilized magnesium-methoxide, J. Solid State Chem. 175 (2003) 278–283, https://doi.org/10.1016/S0022-4596(03)00280-9.

[44] M.L. Addonizio, A. Aronne, C. Imparato, Amorphous hybrid TiO_2 thin films: the role of organic ligands and UV irradiation, Appl. Surf. Sci. 502 (2020), https://doi.org/10.1016/j.apsusc.2019.144095.

[45] V.G. Parale, H. Choi, J. Kim, W. Lee, S.-H. Kim, W.K. Jung, H.-H. Park, Investigation of compound state of SiO_2-TiO_2 aerogel synthesized through controlled sol-gel reaction, J. Alloys Compd. 980 (2024) 173561, https://doi.org/10.1016/j.jallcom.2024.173561.

[46] A. Aronne, E. Marenna, V. Califano, E. Fanelli, P. Pernice, M. Trifuoggi, A. Vergara, Sol-gel synthesis and structural characterization of niobium-silicon mixed-oxide nanocomposites, J. Sol-Gel Sci. Technol. 43 (2007) 193–204, https://doi.org/10.1007/s10971-007-1563-5.

[47] J.A. Wang, O. Novaro, X. Bokhimi, T. López, R. Gómez, J. Navarrete, M.E. Llanos, E. López-Salinas, Characterizations of the thermal decomposition of brucite prepared by sol-gel technique for synthesis of nanocrystalline MgO, Mater. Lett. 35 (1998) 317–323, https://doi.org/10.1016/S0167-577X(97)00273-5.

[48] T. Lopez, I. Garcia-Cruz, R. Gomez, Synthesis of magnesium oxide by the sol-gel method: effect of the pH on the surface hydroxylation, J. Catal. 127 (1991) 75–85, https://doi.org/10.1016/0021-9517(91)90210-U.

[49] N.N. Trukhan, A.A. Panchenko, E. Roduner, M.S. Mel'guno, O.A. Kholdeeva, J. Mrowiec-Białoń, A.B. Jarzebski, FTIR spectroscopic study of titanium-containing mesoporous silicate materials, Langmuir 21 (2005) 10545–10554, https://doi.org/10.1021/la0514516.

[50] F.X. Perrin, V. Nguyen, J.L. Vernet, FT-IR spectroscopy of acid-modified titanium Alkoxides: investigations on the nature of carboxylate coordination and degree of complexation, J. Sol-Gel Sci. Technol. 28 (2003) 205–215, https://doi.org/10.1023/A:1026081100860.

[51] A. Bifulco, F. Tescione, A. Capasso, P. Mazzei, A. Piccolo, M. Durante, M. Lavorgna, G. Malucelli, F. Branda, Effects of post cure treatment in the glass transformation range on the structure and fire behavior of in situ generated silica/epoxy hybrids, J. Sol-Gel Sci. Technol. 87 (2018) 156–169, https://doi.org/10.1007/s10971-018-4710-2.

[52] B. Xu, S. Wei, Y. Liu, S. Zhao, L. Qian, Preparation of an organometallic complex based on phosphonitrile and its flame retardant application in epoxy resin, J. Mater. Res. Technol. 21 (2022) 4921–4939, https://doi.org/10.1016/j.jmrt.2022.11.099.

[53] H. Yan, C. Lu, D. Jing, X. Hou, Chemical degradation of amine-cured DGEBA epoxy resin in supercritical 1-propanol for recycling carbon fiber from composites, Chinese, J. Polym. Sci. 32 (2014) 1550–1563, https://doi.org/10.1007/s10118-014-1519-5.

[54] Z. Zhao, Z. Zhang, C. Sun, M. Xu, B. Li, A novel macromolecular phosphorus-nitrogen containing flame retardant for polycarbonate, Polym. Degrad. Stab. 220 (2024) 110648, https://doi.org/10.1016/j.polymdegradstab. 2023.110648.

[55] R. Rajan, E. Rainosalo, S.K. Ramamoorthy, S.P. Thomas, J. Zavašnik, J. Vuorinen, M. Skrifvars, Mechanical, thermal, and burning properties of viscose fabric composites: influence of epoxy resin modification, J. Appl. Polym. Sci. 135 (2018) 46673, https://doi.org/10.1002/app.46673.

[56] A. Bifulco, R. Avolio, S. Lehner, M.E. Errico, N.J. Clayden, R. Pauer, S. Gaan, G. Malucelli, A. Aronne, C. Imparato, In Situ P-Modified Hybrid Silica–Epoxy Nanocomposites via a Green Hydrolytic Sol–Gel Route for Flame-Retardant Applications, ACS Appl. Nano Mater. 6 (2023) 7422–7435, https://doi.org/10.1021/acsanm.3c00590.

[57] L.K. Lazzari, R.M. Neves, E.F. Kerche, A.B. Vanzetto, H.L. Ornaghi Jr., A.J. Zattera, Biochar from poultry litter as reinforcement used in epoxy-based composites: mechanical and dynamic mechanical properties, Polym. Bull. (2024) 1–16, https://doi.org/10.1007/s00289-023-05128-2.

[58] C. Das, S. Tamrakar, A. Kiziltas, X. Xie, Incorporation of biochar to improve mechanical, thermal and electrical properties of polymer composites, Polymers (Basel). 13 (2021) 2663, https://doi.org/10.3390/polym13162663.

[59] M.K. Umboh, T. Adachi, K. Oishi, M. Higuchi, Z. Major, Mechanical properties of nano-silica particulate-reinforced epoxy composites considered in terms of crosslinking effect in matrix resins, J. Mater. Sci. 48 (2013) 5148–5156, https://doi.org/10.1007/s10853-013-7300-2.

[60] S. Tretsiakova-McNally, P. Joseph, Pyrolysis combustion flow calorimetry studies on some reactively modified polymers, Polymers (Basel). 7 (2015) 453–467, https://doi.org/10.3390/polym7030453.

[61] R. Jian, P. Wang, W. Duan, J. Wang, X. Zheng, J. Weng, Synthesis of a novel P/N/S-containing flame retardant and its application in epoxy resin: thermal property, flame retardance, and pyrolysis behavior, Ind. Eng. Chem. Res. 55 (2016) 11520–11527, https://doi.org/10.1021/acs.iecr.6b03416.

[62] O. Das, N.K. Kim, A.K. Sarmah, D. Bhattacharyya, Development of waste based biochar/wool hybrid biocomposites: flammability characteristics and mechanical properties, J. Clean. Prod. 144 (2017) 79–89, https://doi.org/10.1016/j.jclepro.2016.12.155.

[63] Y. Wang, Y. Zhang, L. Ma, H. Ge, J. Gao, Z. Zhu, Y. Weng, Facile synthesis of phosphorus-containing benzotriazole flame retardant for enhancement of mechanical and fire properties of epoxy resins, Eur. Polym. J. 202 (2024) 112610, https://doi.org/10.1016/j.eurpolymj.2023.112610.

[64] Á. Pomázi, A. Toldy, Development of fire retardant epoxy-based gelcoats for carbon fibre reinforced epoxy resin composites, Prog. Org. Coat. 151 (2021) 106015, https://doi.org/10.1016/j.porgcoat.2020.106015.

[65] H. Vahabi, E. Movahedifar, B.K. Kandola, M.R. Saeb, Flame retardancy index (FRI) for polymer materials ranking, Polymers (Basel). 15 (2023) 2422, https://doi.org/10.3390/polym15112422.

[66] A. Bifulco, D. Parida, K.A. Salmeia, R. Nazir, S. Lehner, R. Stämpfli, H. Markus, G. Malucelli, F. Branda, S. Gaan, Fire and mechanical properties of DGEBA-based epoxy resin cured with a cycloaliphatic hardener: combined action of silica, melamine and DOPO-derivative, Mater. Des. 193 (2020) 108862, https://doi.org/10.1016/j.matdes.2020.108862.

[67] S. Gaan, G. Sun, K. Hutches, M.H. Engelhard, Effect of nitrogen additives on flame retardant action of tributyl phosphate: phosphorus–nitrogen synergism, Polym. Degrad. Stab. 93 (2008) 99–108, https://doi.org/10.1016/j.polymdegradstab.2007.10.013.

[68] H. Gu, J. Guo, Q. He, S. Tadakamalla, X. Zhang, X. Yan, Y. Huang, H.A. Colorado, S. Wei, Z. Guo, Flame-retardant epoxy resin nanocomposites reinforced with polyaniline-stabilized silica nanoparticles, Ind. Eng. Chem. Res. 52 (2013) 7718–7728, https://doi.org/10.1021/ie400275n.

[69] R. Arrigo, P. Jagdale, M. Bartoli, A. Tagliaferro, G. Malucelli, Structure–property relationships in polyethylene-based composites filled with biochar derived from waste coffee grounds, Polymers (Basel). 11 (2019) 1336, https://doi.org/10.3390/polym11081336.

[70] K.A. Salmeia, A. Neels, D. Parida, S. Lehner, D. Rentsch, S. Gaan, Insight into the synthesis and characterization of organophosphorus-based bridged triazine compounds, Molecules 24 (2019) 2672, https://doi.org/10.3390/molecules24142672.

[71] Y. Wang, L. Ma, J. Yuan, X. Yin, H. Wang, C. Cheng, L. Wang, Z. Zhu, Y. Weng, A green flame retardant by elaborate designing towards multifunctional fire-safety epoxy resin composites, React. Funct. Polym. 191 (2023) 105677, https://doi.org/10.1016/j.reactfunctpolym.2023.105677.

[72] K. Barbusiński, A. Parzentna-Gabor, D. Kasperczyk, Removal of odors (mainly H_2S and NH_3) using biological treatment methods, Clean Technol. 3 (2021) 138–155, https://doi.org/10.3390/cleantechnol3010009.

[73] K.-S. Jang, Mineral filler effect on the mechanics and flame retardancy of polycarbonate composites: talc and kaolin, E-Polymers 16 (2016) 379–386, https://doi.org/10.1515/epoly-2016-0103.

[74] L. Zhu, M. Li, S. Zhao, S. Bao, F. Chen, Y. Shangguan, Q. Wu, Q. Zheng, Ultra-high impact PPR composites at low-temperature through enhanced preferential loading of nanoparticles at polymeric interface induced by properly vulcanized rubber dispersed phase, Compos. Sci. Technol. 227 (2022) 109593, https://doi.org/10.1016/j.compscitech.2022.109593.

[75] P. Zielonka, S. Duda, G. Lesiuk, W. Błażejewski, M. Wiśniewska, J. Warycha, P. Stabla, M. Smolnicki, B. Babiarczuk, The effect of flame retardant—aluminum Trihydroxide on mixed mode I/II fracture toughness of epoxy resin, Polymers (Basel). 14 (2022) 4386, https://doi.org/10.3390/polym14204386.